Transition Metal Chemistry (2021) 46:381–390
https://doi.org/10.1007/s11243-021-00455-7

A series of coordination polymers constructed from mixed ligands for highly selective luminescence sensing of Fe^{3+} ions

Yan Wang[1] · Cheng Chen[2] · Huisheng Liu[1] · Dan-Ling Sun[2] · Wei-Wei Cheng[3] · Yun-Shan Xue[2]

Received: 15 January 2021 / Accepted: 18 March 2021 / Published online: 29 March 2021

Abstract

Four coordination polymers, namely $\{[Cd_2(1,4\text{-NDC})_2(dbp)_2]\cdot DMF\}_n$ (1), $\{[Cd(1,4\text{-NDC})(dbp)(H_2O)]\}_n$ (2), $\{[Zn(2,6\text{-NDC})(dbp)(H_2O)]\}_n$ (3), and $\{[Cu(2,6\text{-NDC})(dbp)]\cdot 0.25DMF\cdot 0.2H_2O]\}_n$ (4) (1,4-NDC = 1,4-naphthalenedicarboxylic acid; 2,6-NDC = 2,6-naphthalenedicarboxylic acid; dbp = 4,4′-dimethyl-2,2′-bipyridine), were synthesized under solvothermal conditions by using a mixed-ligand strategy. Single-crystal X-ray diffraction analysis shows that compounds **1** and **2** contain similar 2D layers with $\{4^46^2\}$ topology, while compounds **3** and **4** exist as 1D chain structures, that extend into different 3D supramolecular architectures via H-bonds and interchain π•••π stacking interactions. Title compounds **1-3** exhibit strong emission at 342, 363 and 362 nm, respectively. Moreover, the selective luminescence sensing of compound **1** was investigated, owing to its excellent chemical stability and luminescence properties. Compound **1** shows remarkable fluorescence responses towards Fe^{3+} ions, with a detection limit of 1.0×10^{-5} M, indicating that this compound could sensitively detect trace amounts of Fe^{3+} in aqueous solutions through luminescence quenching.

Introduction

Recently, coordination polymers have attracted intense research interest due to their versatile properties and potential applications in drug delivery [1], catalysis [2, 3], sensing [4–6], magnetism [7–9], gas capture and purification [10–12], etc., as well as their intriguing topologies. Among the extensive well-designed CPs, luminescent coordination polymers (LCPs) exhibit better fluorescence intensity, lifetime, and quantum efficiencies, and provide considerable advantages in nonlinear optics, photocatalysis, white-light emission, and so on [13–18]. Moreover, LCPs can serve as excellent chemical sensors and can be applied in the detection of environmental contaminants at trace levels [19–23]. Fe^{3+} ions are important element in environmental systems and play an irreplaceable role in biological processes, as they are of great importance in oxygen molecule transport and energy transfer in the body. Iron deficiency or accumulation can cause damage to the human body, such as anaemia, and cirrhosis. Thus, design and synthesis of chemosensors with high sensitivity and selectivity for the detection of metal ions have attracted considerable attention. A number of examples have proven that the sensitivity of fluorescence sensing is concerned with the ability of LMOFs to donate electrons because most reported LCP chemosensors follow a mechanism involving electron transfer or energy transfer processes between the CP host and guest analytes, resulting in luminescence quenching [24–26]. Therefore, organic ligands with electron-rich π-conjugated moieties can effectively enhance the luminescence properties of LCPs, which inspired us to construct LCPs by using π-conjugated aromatic ligands here. In this work, we employed 1,4-naphthalenedicarboxylic acid (1,4-NDC) and 2,6-naphthalenedicarboxylic acid (2,6-NDC) in the presence of the auxiliary N-donor linker ligand 4,4′-dimethyl-2,2′-bipyridine (dbp) to construct four coordination polymers, namely $\{[Cd_2(1,4\text{-NDC})_2(dbp)_2]\cdot DMF\}_n$ (1), $\{[Cd(1,4\text{-NDC})(dbp)(H_2O)]\}_n$ (2), $\{[Zn(2,6\text{-NDC})(dbp)(H_2O)]\}_n$ (3), and {[Cu(2,6-NDC)

✉ Yan Wang
B02001@tzu.edu.cn

✉ Yun-Shan Xue
yunshanxue1988@163.com

[1] College of Pharmacy and Chemistry and Chemical Engineering, Taizhou University, Taizhou 225300, People's Republic of China

[2] School of Chemistry and Environmental Engineering, Yancheng Teachers University, Yancheng 224051, Jiangsu, People's Republic of China

[3] School of Chemistry and Bioengineering, Nanjing Normal University Taizhou College, Taizhou 225300, People's Republic of China

(dbp)]·0.25DMF·0.2H_2O]}$_n$ (4). Herein, we report the synthesis, crystal structures and luminescence properties of these compounds. Compound **1** may serve as an efficient sensor for detecting Fe^{3+} ions with good selectivity in aqueous media.

Experimental section

Materials and instruments

The chemical reagents were commercially purchased and used without further purification. Elemental analyses for C, H, and N were carried out on a Perkin-Elmer 240C elemental analyser. Thermogravimetric analysis (TGA) was performed by heating the samples from room temperature to 800 °C at 10 °C/min under a N_2 atmosphere on a NETZSCH STA 449 F5 Jupiter TGA analyser. Powder X-ray diffraction (PXRD) patterns were measured on a Bruker D8 Advance instrument with Cu–Kα radiation ($\lambda = 1.54056$ Å) over the 2θ range of 5–50° at room temperature. Fluorescence measurements of compounds **1-3** were performed on a PerkinElmer LS 55 fluorescence spectrophotometer.

Preparation of compounds 1-4

Synthesis of {[Cd_2(1,4-NDC)$_2$(dbp)$_2$]·DMF}$_n$ (1). A mixture of 1,4-NDC (12 mg, 0.05 mmol), dbp (10 mg, 0.05 mmol), and $CdBr_2·4H_2O$ (25 mg, 0.07 mmol) in DMF (2 mL) and ethanol (1 mL) was sealed in a 25-mL Teflon-lined stainless-steel autoclave at 120 °C for 2 days. Yellow block-like single crystals of **1** were collected in approximately 30% yield based on 1,4-NDC ligand. Elemental analysis for $C_{51}H_{43}Cd_2N_5O_9$, calcd (%): C, 55.95; H, 3.96; N, 6.40. Found (%): C, 55.34; H, 4.19; N, 6.18.

Synthesis of {[Cd(1,4-NDC)(dbp)(H_2O)]}$_n$ (2). A mixture of 1,4-NDC (12 mg, 0.05 mmol), dbp (10 mg, 0.05 mmol), and $CdBr_2·4H_2O$ (25 mg, 0.07 mmol) in DMF (1 mL) and H_2O (2 mL) was sealed in a 25-mL Teflon-lined stainless-steel autoclave at 120 °C for 2 days. Colourless block-like single crystals of **2** were collected in approximately 33% yield based on the 1,4-NDC ligand. Elemental analysis for $C_{24}H_{20}CdN_2O_5$, calcd (%): C, 54.51; H, 3.81; N, 5.30. Found (%): C, 53.89; H, 4.05; N, 5.12.

Synthesis of {[Zn(2,6-NDC)(dbp)(H_2O)]}$_n$ (3). A mixture of 2,6-NDC (12 mg, 0.05 mmol), dbp (10 mg, 0.05 mmol), $Zn(NO_3)_2·6H_2O$ (30 mg, 0.1 mmol), and 150 µL of HNO_3 (2 mol/L) in DMF (1 mL) and H_2O (2 mL) was sealed in a 25-mL Teflon-lined stainless-steel autoclave at 120 °C for 2 days. Colourless block-like single crystals of **3** were collected in approximately 29% yield based on the 2,6-NDC ligand. Elemental analysis for $C_{24}H_{20}ZnN_2O_5$, calcd (%): C, 59.82; H, 4.18; N, 5.81. Found (%): C, 58.93; H, 4.44; N, 5.60.

Synthesis of {[Cu(2,6-NDC)(dbp)]·0.25DMF·0.2H_2O]}$_n$ (4). A mixture of 2,6-NDC (12 mg, 0.05 mmol), dbp (10 mg, 0.05 mmol), $Cu(NO_3)_2·3H_2O$ (24 mg, 0.1 mmol), and 150 µL of HNO_3 (2 mol/L) in DMF (3 mL) was sealed in a 25-mL Teflon-lined stainless-steel autoclave at 120 °C for 2 days. Sky-blue block single crystals of **4** were collected in approximately 25% yield based on the 2,6-NDC ligand. Elemental analysis for $C_{24.75}H_{20.15}CuN_{2.25}O_{4.45}$, calcd (%): C, 61.44; H, 4.20; N, 6.51. Found (%): C, 60.66; H, 4.45; N, 6.28.

X-ray crystallography

The diffraction data of compounds **1-4** were collected using a Bruker D8 QUEST diffractometer equipped with Mo–Kα radiation ($\lambda = 0.71073$ Å). The structures were solved by direct methods and refined using a full-matrix least-squares procedure on F^2 by using the SHELXL package [27]. The hydrogen atoms were generated geometrically and refined isotropically by employing the riding model. All nonhydrogen atoms were refined with anisotropic displacement parameters. In compound **1**, there is positional disorder existing in the naphthyl rings (C45/C46/C47/C48, C50/C52/C55/C56, C41/C42/C43/C44, C49/C51/C53/C54). In compound **2**, two disordered carboxyl (–COO^-) groups of the naphthyl ring were split over two sites. In compound **3**, the disordered O atom of the coordinated water molecule was split over two sites. Because of disorder, some C–C bond distances were restrained. Details of the crystallographic data are listed in Table S1. Selected bond lengths and angles for compounds **1-4** are provided in Table S2.

Results and discussion

Description of crystal structures

Single-crystal X-ray diffraction analyses revealed that compound **1** crystallizes in monoclinic space group $P2_1/c$ and two 1,4-NDC ligands, two dbp ligands, two Cd(II) ions, and two lattice DMF molecules (each having half-occupancies) are present in the asymmetric unit. As shown in Fig. 1, the two Cd(II) ions are six-coordinated in a distorted octahedral geometry, and are surrounded by two nitrogen atoms of one dbp ligand and four oxygen atoms from four different 1,4-NDC ligands. The Cd1 and Cd2 atoms are bridged through four carboxylate groups via bridging bidentate coordination modes to form the dinuclear cluster [$Cd_2(COOR)_4$], and two dbp ligands occupy the remaining coordination sites of the [$Cd_2(COOR)_4$] cluster. The Cd–O bond lengths range from 2.197(4) to 2.378(5) Å and the Cd–N distances

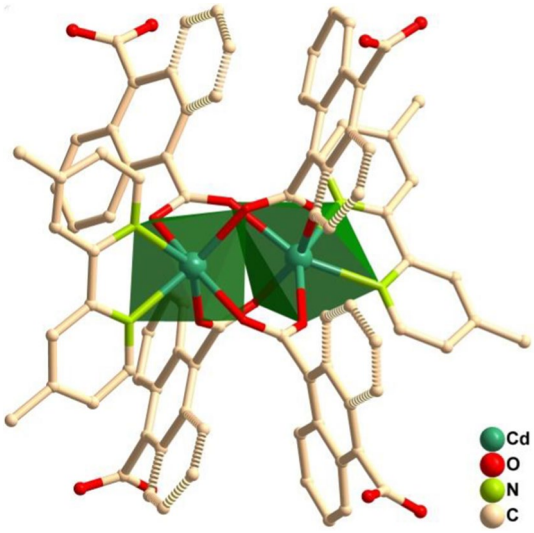

Fig. 1 Coordination environment of Cd centre in compound **1**

range from 2.270(4) to 2.397(4) Å, which are consistent with those in other Cd(II)-based coordination polymers [28]. The $X-\mathrm{Cd}-X$ (X is O or N atom) angles are in the range 68.90(14)–164.09(16)°. Each dinuclear $[Cd_2(COOR)_4]$ unit is connected by four carboxylate groups from four different 1,4-NDC ligands, while the coordinate-unsaturated sites are coordinated by dbp ligands (Fig. 2a). Each adjacent dinuclear unit is connected by two carboxylate groups to construct a 1D linear chain along the *a* or *c* direction (Fig. 2b). In the other direction (*b* direction), the 1,4-NDC ligands are approximately coplanar in the 2D layer, and two dbp ligands have a dihedral angle of 41.079°. Adjacent 2D layers stacked over each other in an ABAB manner along the *c*-axis and further connected into a 3D supramolecular structure through π···π interactions between the pyridine rings, which help stabilize the 3D network (Fig. 3). Topologically, compound **1** can be simplified as a uninodal 4-connected 2D ***sql*** network with a point symbol of $\{4^4 6^2\}$ (Fig. 4).

Single-crystal X-ray diffraction analysis revealed that compound **2** crystallizes in the monoclinic space group $P2_1/n$. The asymmetric unit of **2** is composed of one Cd(II) ion, one 1,4-NDC ligand, one dbp ligand, and one coordinated water molecule. Each Cd(II) ion has a six-coordinate structure, with two nitrogen atoms from one dbp ligand, three oxygen atoms from three 1,4-NDC ligands, and one oxygen from the water molecule, forming a distorted $\{CdN_2O_4\}$ octahedral geometry. The Cd–O bond lengths range from 2.226 (8) to 2.392 (7) Å, and the Cd–N bond lengths range from 2.2949 (17) to 2.3454 (17). Two symmetry-related Cd(II) ions (Cd1 and Cd1A) are further bridged by two carboxyl groups to form a dinuclear metal–carboxylate cluster $[Cd_2(COOR)_4]$ with a Cd···Cd distance of 3.8005 (6) Å (Fig. 5). The 1,4-NDC ligand adopts two coordination modes in compound **2**: one $-COO^-$ group coordinates to one Cd(II) ion in monodentate fashion, and the other $-COO^-$ group links two Cd(II) ions in an μ–O, O bridging mode. Each $[Cd_2(COOR)_4]$ cluster is linked to four other clusters by four 1,4-NDC ligands to generate a 2D framework structure with channel dimensions of 10.7666×10.7666 Å^2 based on the Cd(II) centres (Fig. 6a). In addition, the 2D networks are packed into a 3D supramolecular structure by interlayer π···π stacking interactions between the pyridine rings of the dbp ligands from different layers (Fig. 6b). Topologically, the $[Cd_2(COOR)_4]$ units can be simplified as 4-connected nodes, and the overall motif of compound **2** is a

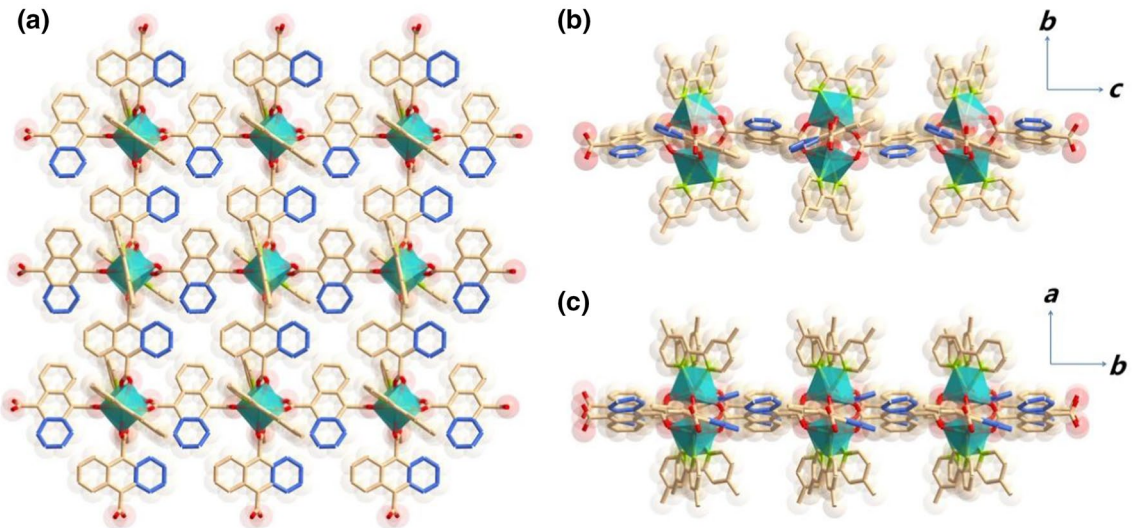

Fig. 2 The crystal structure of compound **1** viewed along different directions

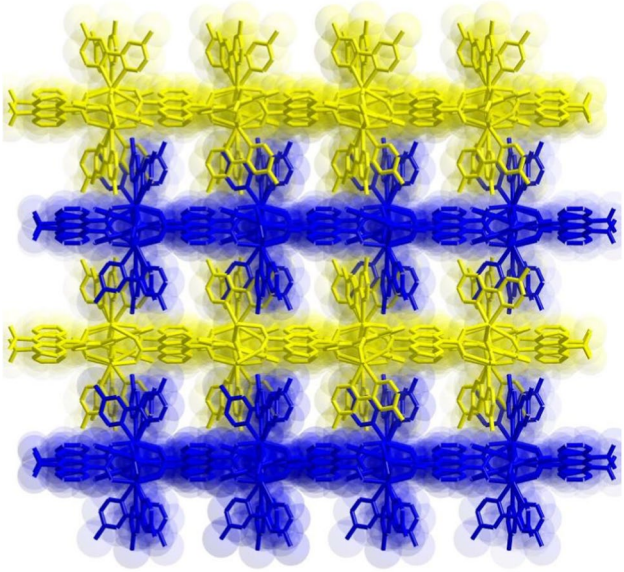

Fig. 3 3D supramolecular structure of compound **1** constructed by π···π interactions and viewed along the *c* direction

uninodal 4-connected ***sql*** 2D net with a point symbol of $\{4^4 6^2\}$ (Fig. 7).

Single-crystal X-ray analysis revealed that compound **3** crystallizes in a triclinic crystal system in the *P*-1 space group, and the asymmetric unit contains one crystallographically independent Zn(II) ion, one 2,6-NDC ligand, one dbp ligand, and one coordinated water molecule. As shown in Fig. 8, each Zn centre adopts a five-coordinate structure, with two oxygen atoms from two monodentate carboxylate groups of two different 2,6-NDC ligands (Zn1–O1 = 1.9572 (14) Å and Zn1–O3 = 2.0746 (15) Å), two nitrogen atoms from one dbp ligand (Zn1–N1 = 2.1040 (17) Å; Zn1–N2 = 2.1641 (18) Å), and one oxygen from the water molecule, forming a distorted square-pyramidal configuration. The $X-\mathrm{Zn}-X$ (*X* is N or O atom) angles range from 76.38 (6) to 165.04 (6)°. Each 2,6-NDC ligand is completely deprotonated and connects two Zn(II) ions in a monodentate coordination mode to form a 1D zigzag chain with an adjacent Zn···Zn separation of 12.847 or 13.330 Å. The dbp ligands and water molecules occupy the remaining coordination sites of the Zn(II) ion. The dangling pyridine rings of the dbp ligand are parallel to each other in the chain, while the dihedral angle between adjacent naphthalene rings ranges from 72.94(4) to 74.10(3)°. Moreover, hydrogen bonds and π···π stacking interactions were observed between pyridine and naphthalene rings from adjacent dbp and 2,6-NDC ligands, which play important roles in the formation of supramolecular structures (Fig. 9).

Compound **4** was obtained via a synthetic route similar to that used to obtain **3**, but the metal salt was changed from Zn(II) to Cu(II). An X-ray diffraction study revealed that compound **4** crystallizes in the *C*2/*c* space group (No. 15), and the asymmetric unit contains one Cu atom (half-occupied), half of a dbp ligand, half of a fully deprotonated 2,6-NDC ligand, and one guest DMF molecule (DMF = *N*,*N*-dimethylformamide). As shown in Fig. 10, the coordination geometry of the Cu atom can be described as square planar and consists of two nitrogen atoms from one chelating dbp ligand (Cu1–N1 = 2.006 (3) Å) and two oxygen atoms from

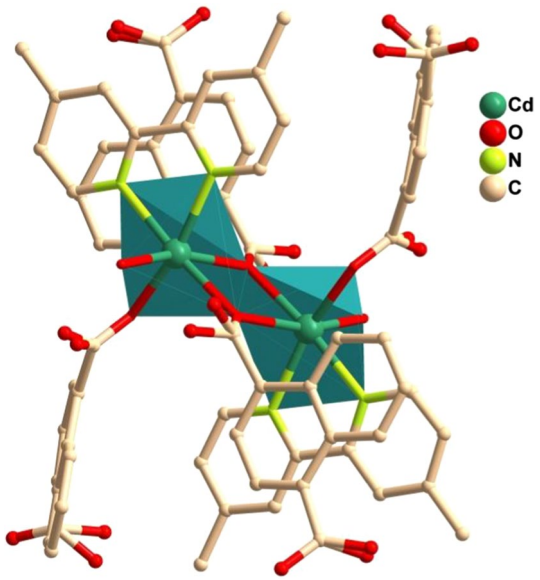

Fig. 5 Coordination environment of the Cd centre in compound **2**

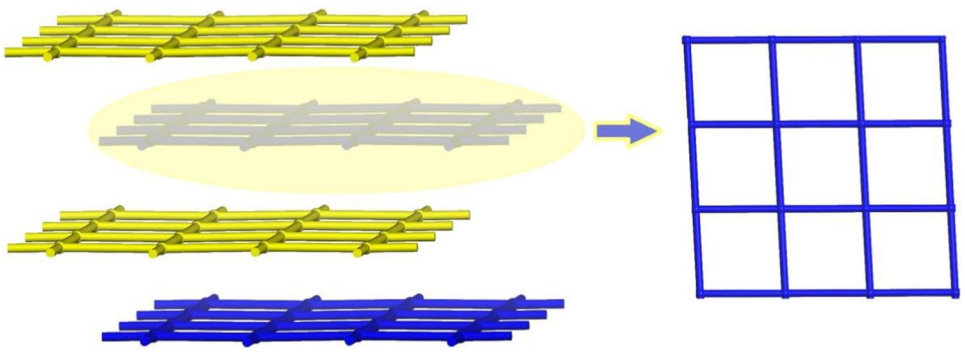

Fig. 4 Schematic representation of the uninodal 4-connected *sql* network in **1**

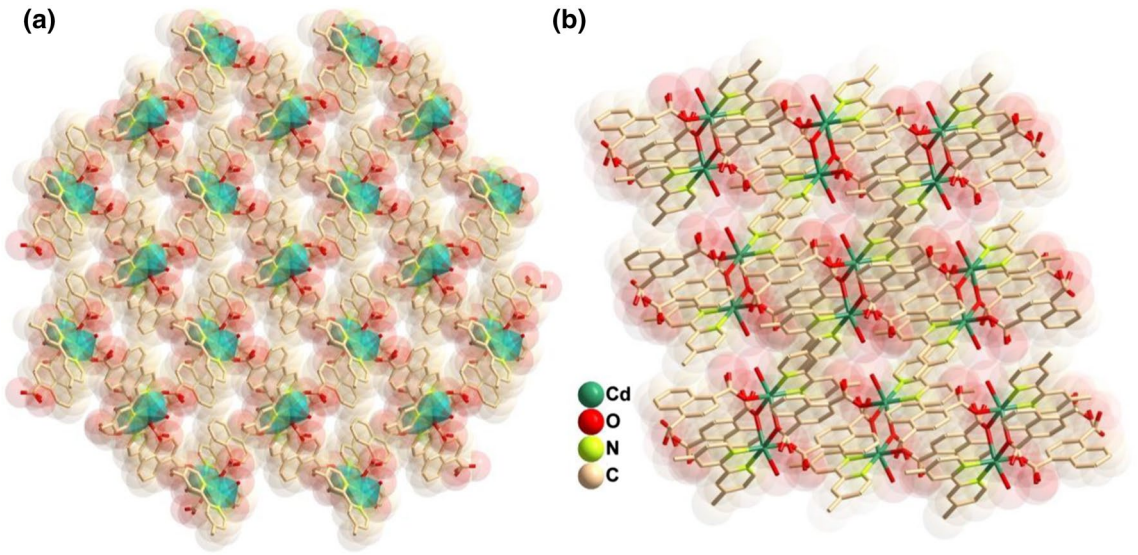

Fig. 6 **a** The 2D structure of compound **2** viewed along the *a* direction; **b** the 3D supramolecular structure of compound **2** constructed by π···π interactions and viewed along the *b* direction

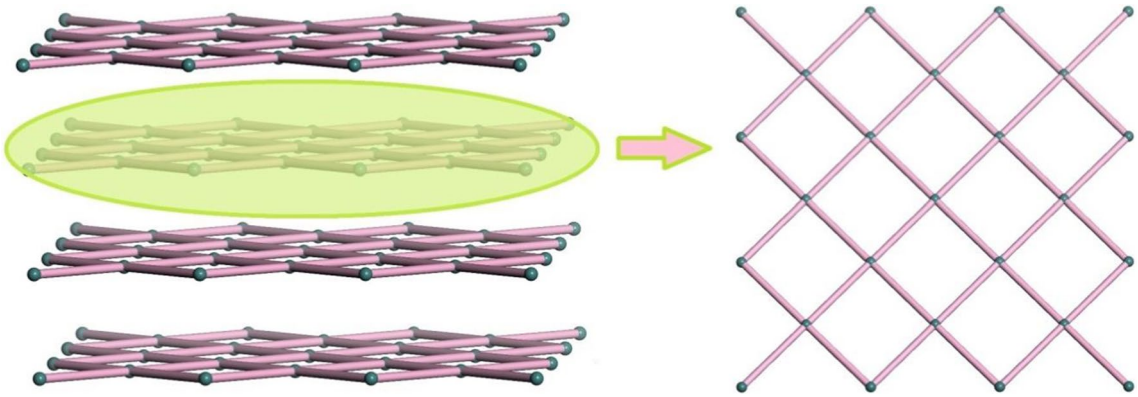

Fig. 7 Schematic representation of the uninodal 4-connected *sql* network in **2**

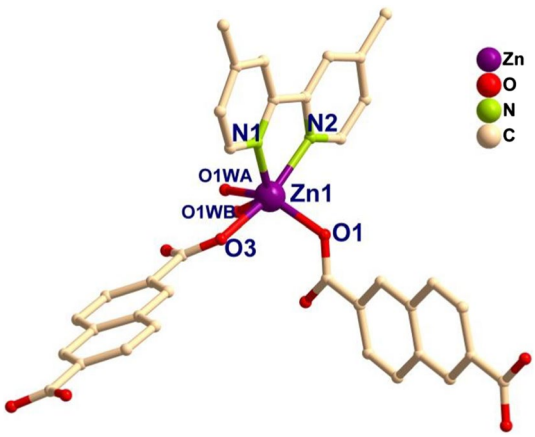

Fig. 8 Coordination environment of the Zn centre in compound **3**

two different 2,6-NDC ligands (Cu1–O2 = 1.970 (2) Å). The bond distances are similar to those reported in the literature [29]. Neighbouring Cu atoms are bridged by a linear 2,6-NDC ligand in a monodentate coordination mode to form an infinite 1D zigzag chain (Cu···Cu distance: 13.0974(7) Å). The terminal dbp ligands occupy the remaining coordination sites of the Cu atoms to form 1D $[Cu(dbp)]_n$ chains and bind alternately on either side of the chains. The chains form an ABC arrangement along *b* axis. All zigzag chains are further extended into a 3D supramolecular architecture by π···π stacking interactions between the pyridyl rings of different dbp ligands, which play an important role in the formation of the overall structure (Fig. 11).

Compounds **1-4** are constructed from the N-donor ancillary ligand 4,4′-dimethyl-2,2′-bipyridine (dbp) and different

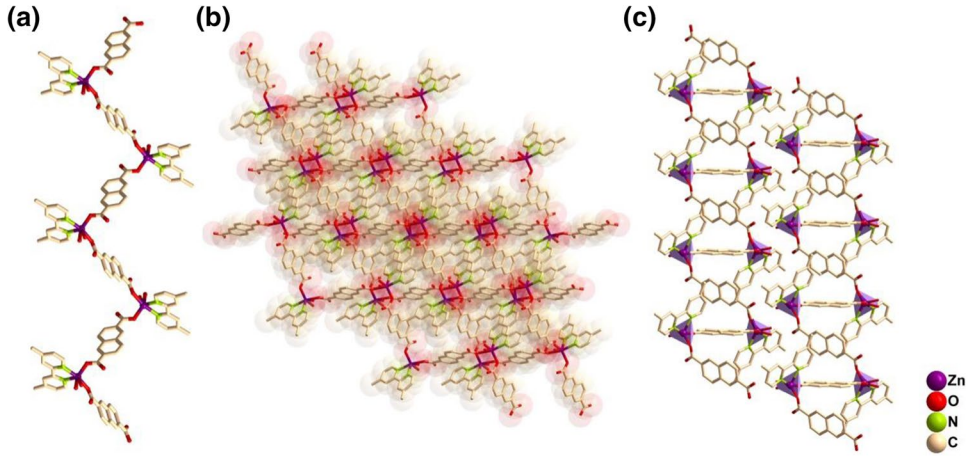

Fig. 9 **a** A drawing showing the 1D chain; **b** and **c** 3D supramolecular structure of compound **3** stacked by H-bonding and π···π interactions viewed along the *c*- and *a*- axes, respectively

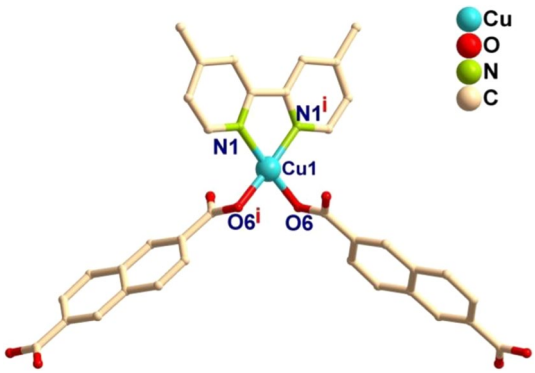

Fig. 10 Coordination environment of the Cu centre in compound **4**

O-donor ligands i.e. 1,4-naphthalenedicarboxylate (1,4-NDC) and 2,6-naphthalenedicarboxylic acid (2,6-NDC). Compounds **1** and **2** show different 2D layer structures with *sql* topology; **3** and **4** form 1D waved chains. It is known that many factors can affect nucleation and crystal growth in the formation of coordination polymers, such as solvent, temperature, pH values, starting concentrations of the reactants and counteranions. In the aforementioned structures, compounds **1-2** have been synthesized under the same synthetic conditions but with different solvents (proportion and type), i.e. DMF/EtOH (v/v = 2/1) and DMF/H_2O (v/v = 1/2), respectively. Thus, the solvent plays a crucial role in the formation of different crystal structures. The resulting compounds **1**

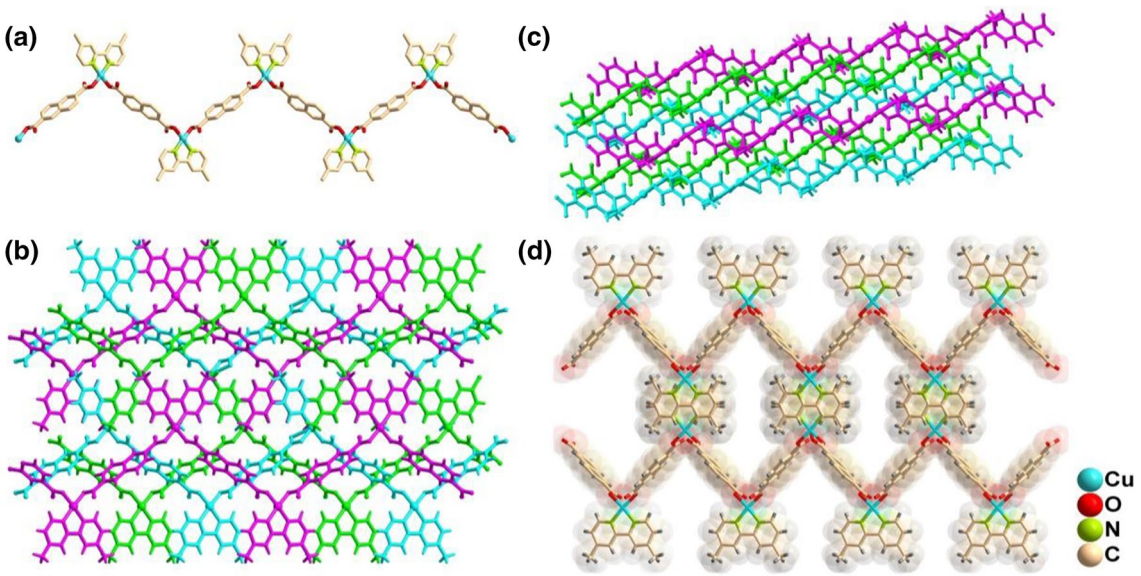

Fig. 11 **a** A drawing showing the 1D chain; **b**, **c** and **d** 3D supramolecular structure stacked by H-bonding and π···π interactions viewed along the *a*-, *b*- and *c*- axes, respectively

and **2** have similar crystal structures, while the coordination modes for the 1,4-NDC ligands are different in their secondary building units (SBUs). In compound **1**, 1,4-NDC ligands coordinate to the $[Cd_2(COOR)_4]$ SBU in a bidentate manner via its two carboxylate groups, and the 1,4-NDC ligands are approximately coplanar. Two dbp ligands occupy the remaining coordination sites of the $[Cd_2(COOR)_4]$ cluster with a dihedral angle of 41.079°, and are perpendicular to the 1,4-NDC 2D plane. In compound **2**, the 1,4-NDC ligands coordinate to the $[Cd_2(COOR)_4]$ SBU in monodentate mode and m–O, O bridging modes. Each SBU is linked to four other clusters by four 1,4-NDC ligands to form a 2D layer structure similar to that of compound **1**. Slightly different from compound **1**, two opposite dbp molecules in the $[Cd_2(COOR)_4]$ SBU are nearly parallel to each other. Moreover, it is of interest to note that the anion (Br^-) of the metal salt ($CdBr_2$) does not participate in formation of the structure in our case but influences the formation of the resulting crystals. We used $CdBr_2$ and $Cd(NO_3)_2$ as metal salts to perform comparative experiments under the same reaction conditions, and the resulting products had did not form crystals in the presence of the metal nitrate $Cd(NO_3)_2$. Compounds **3** and **4** exhibit similar 1D chains, which extend into different 3D supramolecular architectures via H-bonds and/or π···π stacking interactions. The 2,6-NDC ligand (2,6-naphthalenedicarboxylic acid) adopts a monodentate coordination mode to construct a 1D zigzag chain in compounds **3-4**. This structure may be derived from the metal centres, i.e. Zn(**3**) and Cu(**4**), which exhibit a five-coordinate distorted square-pyramidal configuration and a four-coordinate square planar configuration, respectively. By comparing the structures of **1-4**, it can be clearly inferred that rigid ligands more easily form rigid structural and reduce structure uncertainty, while the addition of an auxiliary ligand could provide greater flexibility than a single ligand.

Thermal stability of compounds 1-4

The phase purity of as-synthesized compounds **1-4** was confirmed by powder X-ray diffraction (Fig. S1–S4). Thermogravimetric analysis (TGA) was performed in the temperature range of 20–800 °C to investigate the thermal stability of compounds **1-4**. As seen from the TG curve (Fig. 12), compound **1** displayed a weight loss of 6.54% at 25–175 °C, corresponding to the loss of the guest DMF molecule (calcd 6.68%). Upon further heating, compound **1** remained stable at temperatures of up to 290 °C. Above this temperature, the compound decomposed with an abrupt weight loss. Compound **2** exhibited a weight loss of 3.15% at 25–130 °C, contributing to the loss of coordinated water molecules (calcd 3.41%). Upon further heating, compound **2** remained stable up to 350 °C. Above this temperature, the compound decomposed with an abrupt weight loss. For compound **3**, the TGA

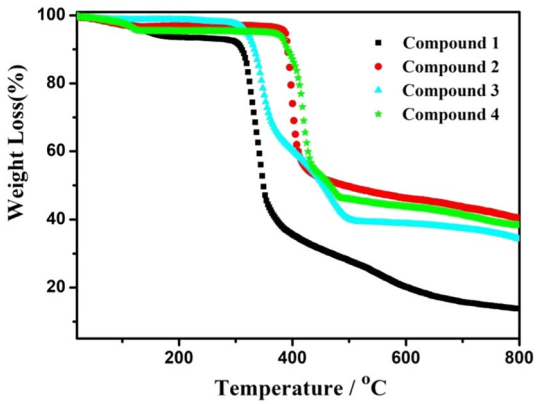

Fig. 12 TG curves of compounds **1–4**

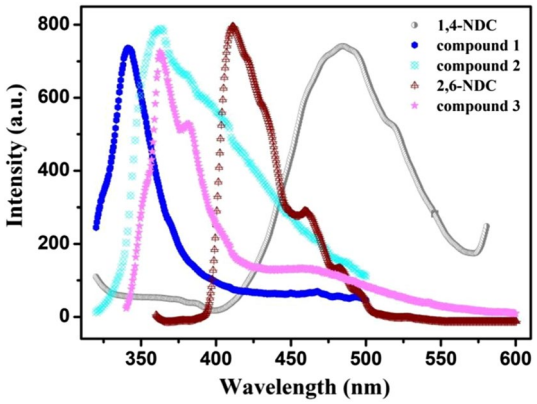

Fig. 13 Solid-state emission spectra of compounds **1–3** and free ligands

curve showed a slow weight loss of 3.35% between 25 and 310 °C, contributing to the loss of coordinated water molecules (calculated 3.74%). Further heating resulted in release of the coordinated organic ligand and the collapse of the lattice structure. Compound **4** exhibited a weight loss of 4.66% at 25–140 °C, corresponding to the release of guest DMF molecules (calcd 4.52%). As seen from the TG curve, compound **4** remained stable until 350 °C with no weight loss. Upon further heating, the lattice structure collapsed, and the organic ligand decomposed with an abrupt weight loss.

Luminescence properties

The luminescence properties of the free ligands 1,4-NDC and 2,6-NDC and compounds **1-3** were examined at room temperature in the solid state. As shown in Fig. 13, the emission spectra of compounds **1-2** exhibit strong emission at 342 nm (λ_{ex} = 305 nm) and 363 nm (λ_{ex} = 335 nm), with a blueshift compared to the spectrum of the free ligand 1,4-NDC (λ_{em} = 485 nm). Upon excitation of compound **3** at

328 nm, the corresponding bands are observed at 362 nm, which are similar to those of the free 2,6-NDC ligand (λ_{em} = 410 nm). The emission peaks of the free ligands 1,4-NDC and 2,6-NDC can be assigned to $\pi/n \rightarrow \pi^*$ electron transitions [30, 31]. Considering the d^{10} electronic configuration of Zn(II)/Cd(II) cations, the emission peaks of compounds **1-3** do not correspond to either ligand-to-metal charge transfer (LMCT) or metal-to-ligand charge transfer (MLCT) transitions. Thus, the emissive behaviours of **1-3** can be attributed to intra-ligand charge transfer.

Detection of metal ions

Considering the excellent luminescence properties and good stabilities of compound **1** in water, the potential sensing and detection abilities of **1** for metal ions in aqueous solution were explored. Further investigation was performed by using a 5 mg finely ground sample of compound **1** dispersed into a 3.0 mL 0.005 mol/L $M(NO_3)_n$ aqueous solution (M = Li^+, Na^+, Ag^+, Ca^{2+}, Mg^{2+}, Zn^{2+}, Cd^{2+}, Co^{2+}, Cu^{2+}, Pb^{2+}, Cr^{3+}, Al^{3+}, Fe^{3+}). As seen in Fig. 14, the different metal ions display distinct quenching behaviour, and Fe^{3+} exhibits extremely significant quenching effects (97.1% reduction in intensity), which prompted us to investigate the sensing sensitivity of **1** for Fe^{3+}.

Anti-interference experiments were conducted by adding Fe^{3+} into the suspension of compound **1** containing various metal ions. As shown in Fig. 15, the intensities of **1** in the Fe^{3+}-M mixed system (M = Li^+, Na^+, Ag^+, Ca^{2+}, Mg^{2+}, Zn^{2+}, Cd^{2+}, Co^{2+}, Cu^{2+}, Pb^{2+}, Cr^{3+}, Al^{3+}) show only minor changes compared to that of **1** exposed to Fe^{3+} ions. These results reveal that **1** shows good anti-interference in the detection of Fe^{3+}. Then, concentration-dependent

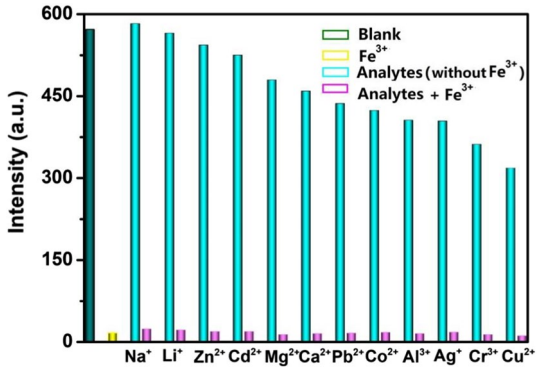

Fig. 15 Luminescence intensity of compound **1** with different metal ion solutions containing Fe^{3+} ions

luminescence experiments were performed with a series of **1**-Fe^{3+} suspensions to further explore the sensitivity of **1** towards Fe^{3+}. As shown in Fig. 16, the emission intensity of compound **1** gradually decreased with increasing concentrations of Fe^{3+}.

The relationship between the concentration of Fe^{3+} and the quenching efficiency was evaluated quantitatively by employing the Stern–Volmer (S–V) equation ($I_0/I = K_{sv}[Fe^{3+}] + 1$). Here, I_0 and I represent the luminescence intensities of the suspension without and with the addition of Fe^{3+}, respectively; K_{sv} is the quenching rate constant; and [Fe^{3+}] refers to the concentration of Fe^{3+} ions in aqueous solution. As shown in Fig. 17, the concentration of Fe^{3+} ions and I_0/I show a good linear correlation at low concentrations, and the K_{sv} value was calculated to be 1.62×10^4 M^{-1}. The related detection limit (LOD) for Fe^{3+} ions was calculated to be 1.0×10^{-5} M by the formula

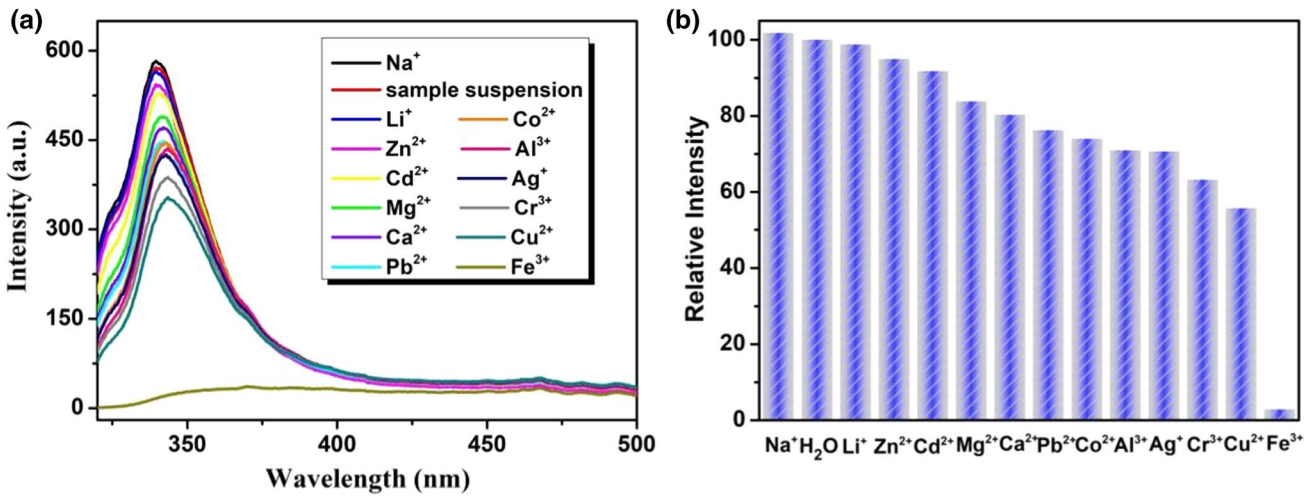

Fig. 14 **a** Photoluminescence spectra of compound **1** after the samples were dispersed in 0.005 mol/L $M(NO_3)_n$ aqueous solutions; **b** the relative intensity of compound **1** towards metal ions in aqueous solution

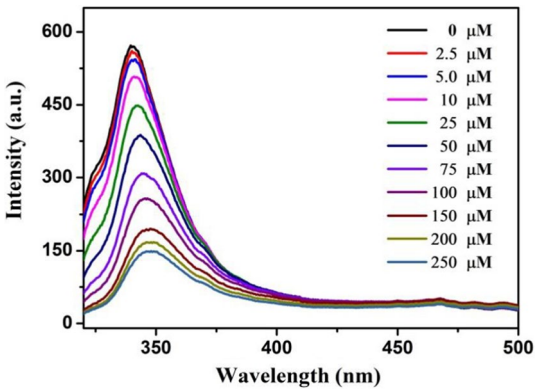

Fig. 16 Luminescence intensity of compound **1** upon exposure to different concentrations of Fe^{3+}

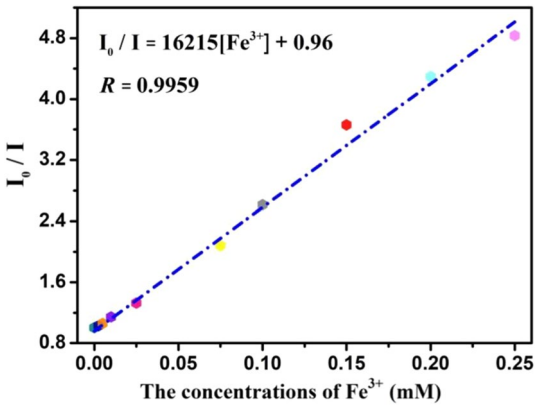

Fig. 17 Stern–Volmer plot of compound **1** versus Fe^{3+} concentrations

$3\delta/K_{sv}$, where σ is the standard deviation for five luminescence tests using a blank solution.

Conclusion

In this paper, we synthesized and structurally characterized a series of coordination polymers by employing the rigid ligands 1,4-naphthalenedicarboxylic acid (1,4-NDC) and 2,6-naphthalenedicarboxylic acid (2,6-NDC) and the N-donor linker 4,4′-dimethyl-2,2′-bipyridine (dbp). Compounds **1-2** exhibited 2D layer architectures with ***sql*** topology. Compounds **3-4** adopted 1D waved chain structures and extended into different 3D supramolecular structures. Luminescence sensing exploration revealed that compound **1** possesses excellent performance in sensing Fe^{3+} ions in aqueous solution, and the detection limit was 1.0×10^{-5} M.

Supplementary Information The online version contains supplementary material available at https://doi.org/10.1007/s11243-021-00455-7.

Acknowledgements This work was financially supported by the Natural Science Foundation of the Jiangsu Higher Education Institutions of China (Grant No. 20KJB150009).

References

1. Chen X, Tong R, Shi Z, Yang B, Liu H, Ding S, Wang X, Lei Q, Wu J, Fang W (2018) ACS Appl Mater Interfaces 10:32328–32337
2. Vellingiri K, Philip L, Kim KH (2017) Coordin Chem Rev 353:159–179
3. Park HD, Dinca M, Roman-Leshkov Y (2018) J Am Chem Soc 140:10669–10672
4. Zuo Y, Yang J, Chen C, Xue YS, Zhang J (2020) Acta Crystallogr C 76:1076–1084
5. Chen Z, Yang J, Cheng WW, Huang J, Yang D, Xue YS, Wu XH (2020) Transit Metal Chem 45:121–128
6. Chen XB, Qi CX, Xu YB, Li H, Xu L, Liu B (2020) J Mater Chem C 8:17325–17335
7. Lee J (2020) CrystEngComm 22:8081–8087
8. Wei XQ, Shao D, Xue CL, Qu XY, Chai J, Li JQ, Du YE, Chen YQ (2020) CrystEngComm 22:5275–5279
9. Huang H, Gao W, Zhang XM, Zhou AM, Liu JP (2019) CrystEngComm 21:694–702
10. Zarate JA, Dominguez-Ojeda E, Sanchez-Gonzalez E, Martinez-Ahumada E, Lopez-Cervantes VB, Williams DR, Martis V, Ibarra IA, Alejandre J (2020) Dalton Trans 49:9203–9207
11. Xu WQ, He S, Lin CC, Qiu YX, Liu XJ, Jiang T, Liu WT, Zhang XL, Jiang JJ (2018) Inorg Chem Comm 92:1–4
12. Kim KC (2018) J Organomet Chem 854:94–105
13. Nagarkar SS, Desai AV, Ghosh SK (2016) CrystEngComm 18:2994–3007
14. Yang J, Wang Z, Hu KL, Li YS, Feng JF, Shi JL, Gu JL (2015) ACS Appl Mater Interfaces 7:11956–11964
15. Hu YL, Ding M, Liu XQ, Sun LB, Jiang HL (2016) Chem Commun 52:5734–5737
16. Xu BW, Niu RJ, Liu Q, Yang JY, Zhang WH, Young DJ (2020) Dalton Trans 49:12622–12631
17. Zareba JK, Nyk M, Janczak J, Samoc M (2019) ACS Appl Mater Interfaces 11:10435–10441
18. Zhang DM, Xu CG, Liu YZ, Fan CB, Zhu B, Fan YH (2020) J Solid State Chem 290:121549
19. Hao SY, Hou SX, Hao ZC, Cui GH (2018) Spectrochim Acta A 189:613–620
20. Liu D, Dong G, Wang X, Nie F, Li X (2020) CrystEngComm 22:7877–7887
21. Li Z, Zhan Z, Hu M (2020) CrystEngComm 22:6727–6737
22. Yang DD, Lu LP, Zhu ML (2020) CrystEngComm 22:5207–5217
23. Wang JJ, Wu FF, Su N, Li PP, Wang SY, Ma HY, Li YW, Yu MH (2020) CrystEngComm 22:4650–4664
24. He HM, Song Y, Sun FX, Bian Z, Gao LX, Zhu GS (2015) J Mater Chem A 3:16598–16603

25. Song XZ, Song SY, Zhao SN, Hao ZM, Zhu M, Meng X, Wu LL, Zhang HJ (2014) Adv Funct Mater 24:4034–4041
26. Xu N, Zhang Q, Zhang G (2019) Dalton Trans 48:2683–2691
27. Sheldrick GM (2015) Acta Crystallogr Sect C 71:3–8
28. Chen ZL, Dong Y, Liu QW, Bian RR, Cheng WW, Xue YS, Liu MP (2019) Transit Metal Chem 44:445–454
29. Xue YS, He Y, Ren SB, Yue Y, Zhou L, Li YZ, Du HB, You XZ, Chen B (2012) J Mater Chem 22:10195–10199
30. Lakowicz JR (2006) Principles of fluorescence spectroscopy, 3rd edn. Springer, Berlin
31. Valeur B (2002) Molecular fluorescence: principles and application. Wiley-VCH, Weinheim